Constant Mean Curvature Surfaces Derived from Delaunay's and Wente's Examples

K. Große-Brauckmann * and K. Polthier **

[1] Mathematisches Institut, Universität Bonn
[2] Fachbereich Mathematik, Technische Universität Berlin

Summary. We show how Wente tori and Delaunay surfaces can be used as building blocks to construct new surfaces of constant mean curvature. In a first part we give examples of periodic Wente tori and Wente tori with Delaunay ends. In a second part we study all embedded Delaunay-like surfaces with a fixed number of ends and some given reflectional symmetry.

1. Introduction

Constant mean curvature (CMC) surfaces arise as interfaces in many physical problems, and have been studied since more than a century. Nevertheless only in the last decades the set of known constant mean curvature surfaces has been broadly enlarged by a number of breakthroughs. The most famous one was Wente's surprising discovery of a compact surface other than the sphere: in 1984 Wente found CMC tori [18], and Abresch determined all tori with planar curvature lines [1]. By the classification of Pinkall, Sterling [17], and Bobenko [2] it turned out that CMC tori can be described explicitly in terms of theta functions. The class of tori is special in that it forms an integrable system.

An entirely different method, an analytic gluing construction, was used by Kapouleas to construct compact CMC surfaces of genus $g \geq 2$ [9] [10] and surfaces with $k \geq 3$ ends for each genus [8]. A *gluing construction* means to search new surfaces close to a collection of some previously known surfaces. In the case of [10] the known surfaces are Wente tori. In the other cases they are the simply periodic CMC surfaces of revolution determined by Delaunay in 1841. Mathematically the gluing is an application of the implicit function theorem. To have sufficient control of the surfaces to be glued together Kapouleas takes them almost degenerate: he restricts to Wente tori with many lobes and Delaunay surfaces with thin necks. Then both torus lobes and Delaunay bulges are rather spherical, and thus all of Kapouleas' surfaces are a collection of almost spheres joined with the appropriate small handles. In [15] work in progress is announced on gluing constructions using the other extreme of the Delaunay surfaces, the cylinder; again small handles join the almost cylinders. Thus in all cases gluing constructions yield surfaces close

* Supported by SFB 256 at Universität Bonn
** Partially supported by SFB 288 at Technische Universität Berlin

to the degenerate boundary of the set of all CMC surfaces; the boundary is reached when the handles pinch off. This means gluing constructions provide sets in a neighbourhood of the boundary of the moduli space.

Lawson found another method to construct CMC surfaces [14]. This *conjugate surface method*, in its extensions due to Karcher [11] and the first author [4], allows to construct rather explicit surfaces allover the moduli space. A fundamental piece of a CMC surface is constructed by finding an appropriate 'conjugate' minimal surface in the 3-sphere S^3. The entire CMC surface is generated by planar reflections of the fundamental piece. For many surfaces the reflections only close up if a *period problem* is solved. With the conjugate surface construction, this arises in the form that two boundary symmetry curves of the fundamental patch must lie in the same (symmetry) plane; but it is merely known that the two symmetry planes are parallel. The construction involves parameters determining the distance of two such parallel planes, and we must prove existence of a special parameter value such that the distance is zero.

A rigorous mathematical proof has not been found for the general period problem, but with the algorithm of Oberknapp and the second author [16] it is now possible to investigate the period problem numerically. The algorithm defines a discrete version of the conjugate surface construction. It is included with the mathematical visualization environment GRAPE from the Sonderforschungsbereich 256 of the University of Bonn. The convenient visualisation of CMC surfaces provided by this program led to new insight in the geometry of CMC surfaces; in previous work we used the algorithm to show that the conjugate surface construction yields explicit compact CMC surfaces [6] [7].

In the present paper we apply the algorithm to two problems. In Section 3. we combine the essential building blocks, Wente tori and Delaunay surfaces, to new surfaces. In particular we include Wente tori and Delaunay surfaces into a single surface. Our examples serve as an illustration of how the gluing idea applies to surfaces away from the degenerate case. In fact, for many of the surfaces presented it is essential that we are far away from the degenerate situation; for instance the periodic surfaces we derive from Wente tori arise only from tori with few lobes. The reader will get an idea of the many other modifications of CMC surfaces which seem feasible.

In Section 4. our approach is different. First we study the entire class of three-ended embedded CMC surfaces with two equal ends. These surfaces, which we call *isosceles triunduloids*, are basically triple junctions with ends. Following a suggestion of R. Kusner we then investigate surfaces which arise from the symmetric composition of such building blocks: *rhombic 4-unduloids* decompose into two isosceles triple junctions and *k-unduloids of genus 1* contain k of them. Again we can deal with the entire classes of these surfaces. In other words we know the respective moduli spaces, and not just some neighbourhood of their boundaries. This is the first global information on spaces of embedded surfaces with genus $g \geq 0$ and $k \geq 3$ ends. Although our

results deal only with sufficiently symmetric surfaces they provide evidence that e.g. the general moduli spaces of the genus 0 surfaces with k ends are connected. Thus a genus 0 CMC surface with k ends seems to be deformable to any other CMC surface with k ends through CMC surfaces.

2. Delaunay Unduloids and Wente Tori

Color Plate A.1 (p. 18 in the Appendix) depicts two bubbles of an *unduloid*, i.e. an embedded CMC surface with two ends. The 1-parameter family of these simply periodic surfaces was determined by Delaunay [3] using the property that they can be generated as surfaces of revolution. Only much later it was seen that there are no further embedded surfaces with two ends [12]. As the Latin root *unda* indicates the generating curve resembles a sequence of waves. The radius of the waist parameterizes the family and ranges from 0, when the surfaces degenerate to a string of touching spheres, to $\frac{1}{2}$, which is attained by the cylinder. There are further non-embedded surfaces of revolution, the *nodoids*, which could similarly be used in constructions.

An embedded end of a CMC surface is asymptotically a Delaunay unduloid [12]; this means that the distance to some unduloid tends to 0 as the end extends to infinity. Thus we can include embedded ends into the following definition:

Definition 2.1. *The smallest radius $\rho \in (0, 1/2]$ is called the* necksize *of a Delaunay unduloid. For embedded ends of* CMC *surfaces the term necksize refers to the asymptotic value of the smallest neck radius, likewise the axis to the asymptotic axis.*

Kusner's balancing formula [12] states for a surface with k embedded ends of necksize ρ_i and with (outward oriented) axis $v_i \in \mathsf{S}^2$ that

$$\sum_{i=1}^{k} 2\pi\rho_i(1-\rho_i)v_i = 0. \tag{2.1}$$

The summand $2\pi\rho(1-\rho)v$ is called the *force* of an unduloid end. More generally, each handle of a CMC surface can be associated a force vector by an integral expression; then Kusner's *balancing formula* says that the sum of the forces of all handles emanating from a given bubble vanishes. The force is in fact the physical force effective on a wire frame bounding a soap bubble film.

Another prototypical CMC surface is the *Wente torus*. Color Plate A.1 displays a Wente torus with 3 lobes. Its geometry might seem difficult to understand, but we only use the following property which is apparent from the image: the torus can be generated by reflection from a simply connected piece. This piece is a rectangle with four planar symmetry arcs as boundary. We can glue two copies of the rectangle along a pair of opposite boundary arcs together. Two pairs of S-shaped curves then complete to 'figure 8'-curves.

These figure 8 curves are the vertical thickend curves in color plate A.1. They have one large loop running around the lobe as well as one small loop. Since only two figure 8 curves bound the glued two rectangles they are topologically a cylinder of finite length, $\mathsf{S}^1 \times [0,1]$. However, unlike the cylinder the bounding curves are contained in tilted and not parallel planes, so that successive reflection in these planes leads to a closed surface provided the angle between the planes is rational. In the simplest case k doubled rectangles combine to a k-lobed torus. The lobes are almost spheres, and indeed the fundamental rectangle forms two quarter spheres, so that $2k$ copies form k spheres.

The 3- and 4-lobed Wente tori are unique, but for larger k there are many geometrically different Wente tori. All have *dihedral symmetry of order* k, denoted by D_k, i.e. they have the symmetries of a planar k-gon in 3-space. They have a further reflectional symmetry plane in the plane of the k-gon, so that the entire symmetry group is $D_k \times \mathbf{Z}_2$. It is convenient to call the plane of the k-gon *horizontal*, its normal *vertical*.

3. Modifying the Wente Torus

3.1 Periodic Wente Tori

An obvious attempt to modify the Wente torus would be to attach small half handles horizontally at the outermost positions of all bubbles such that the handles have boundary 'circles' in vertical planes. By planar reflection in these planes we would obtain doubly periodic surfaces for the 3-, 4- and 6-lobed tori. Using spherical trigonometry, it can be shown that such surfaces do not exist.

Nevertheless we can join Wente tori horizontally. To do so we remove from each lobe the outer hemisphere. We can slightly deform the torus so that the bounding 'circles' become symmetry lines and admit reflection of the torus to a doubly periodic CMC surface. Presumably the bounding circle has vanishing force. On the other hand a small handle has a non-zero force, and the above non-existence statement can be interpreted to say that any force pulling the lobes of the Wente torus apart would pop the torus.

In Figure 3.1 we show the result for the 3-lobed torus. There is still a period problem involved as for the standard Wente torus, but this is different from the periodicity properties of the constructed periodic surface. We solved the period problem numerically, and obtained doubly periodic 3- and 4-lobed Wente tori; similarly we expect that we can modify the two 6-lobed Wente tori to become doubly periodic.

Experimental Result 1. *For* $n = 3, 4$ *there exist doubly periodic* CMC *surfaces whose fundamental cell is a torus with symmetry* $D_n \times \mathbf{Z}_2$ *contained in a triangular or quadratic prism, respectively.*

Proof. For the conjugate surface construction we must specify a polygonal boundary contour in S^3. This contour is easily derived from the contour of a Wente torus by cutting off parts of the contour with a spherical geodesic of length $\frac{\pi}{2}$ and orthogonal to the two adjacent arcs. For a given number of lobes, there is one free parameter in the family of such contours, and it is used to kill the period numerically.

A similar recipe should work with every other lobe of an even-lobed torus. Reflection leads to doubly periodic tori for suitable 6-, 8-, and 12-lobed tori. The 4-lobed torus gives a simply periodic surface, and we confirmed numerically that the period problem can be solved in this case; see Figure 3.1.

Experimental Result 2. *There is a simply periodic* CMC *surface with translational fundamental domain of genus* 1 *and symmetry* $D_4 \times \mathbf{Z}_2$.

A different idea is to insert vertical handles, one on top and bottom of each lobe. Here there is no problem with the soap film forces since they balance in each bubble provided we take the two opposite handles of the same size. Their only impact is to stretch the lobes vertically while keeping the torus center almost unchanged. Vertical handles work for a range of necksizes, and indeed we observed a family of surfaces with varying necksizes. This should give simply periodic surfaces derived from Wente tori with any number of lobes. Figure 3.1 displays our numerical result for the 3-lobed torus.

Experimental Result 3. *There is a continuous family of simply periodic surfaces whose degenerate limit is as follows:* 3*-lobed Wente tori are stacked vertically over each other such that adjacent tori touch in three points.*

3.2 Wente Tori with Delaunay Ends

Once we know that each lobe of a Wente torus behaves like a sphere when modified equally at top and bottom we can try further modifications. For example we attach Delaunay unduloids at the top and bottom position of each bubble. We conducted experiments with the 3-lobed torus and succeeded to solve the period problem, see Color Plate A.1 (p. 18 in the Appendix).

Experimental Result 4. *There is a continuous family of genus* 1*surfaces with six unduloids ends and symmetry* $D_3 \times \mathbf{Z}_2$. *The unduloid ends have parallel axes, and the same necksize* $0 < \rho < \rho_0$. *When* ρ *tends to* 0, *the surfaces converge to a* 3*-lobed Wente torus with six strings of spheres attached.*

An obvious problem is posed by the last two results, namely to determine the entire family, in particular to determine the degenerate limit at the other end of the family. Although there is no proof that the family can only degenerate with a curvature blow-up, this behaviour, in form of pinched-off handles, is displayed by all known examples and proven for the embedded

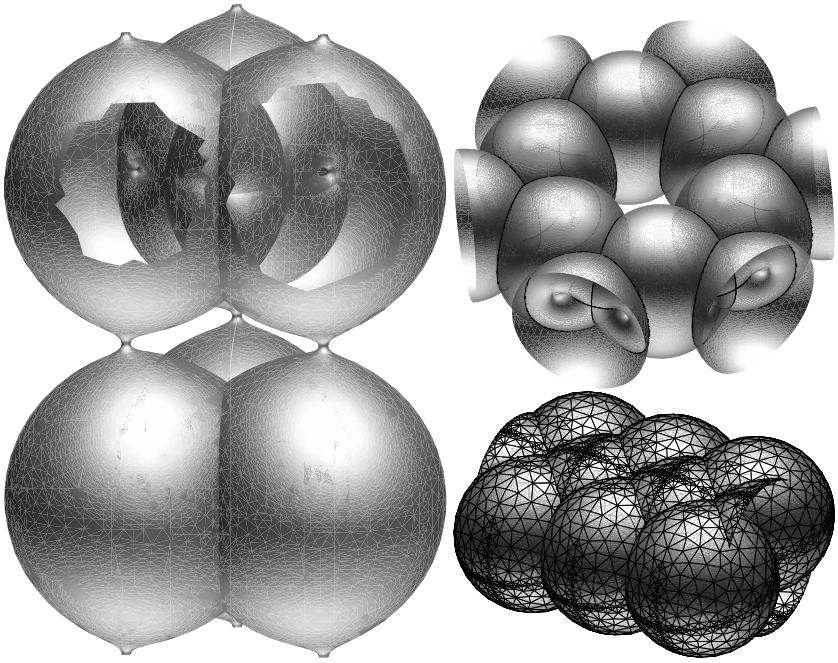

Fig. 3.1. *Modifications of the Wente torus to produce periodic* CMC *surfaces with genus 1 fundamental domain. In the left image the torus is modified to have six small handles at vertical positions. The reflected surface is a simply periodic stack of Wente tori. The image shows two of the tori, with the upper one opened to give view to the interior of the surface. – The top right surface is doubly periodic and obtained from the 3-lobed torus, whereas the singly periodic surface depicted in the third image was obtained from a modified 4-lobed torus. For the two right surfaces the modification is not far away from removing the outer halves of lobes of the standard Wente tori.*

case [13]. In any case, there should be no difference for the two cases of one handle or an entire unduloid end.

To conclude this section we mention a few modifications of Wente tori which would generalize our results:

- Simply periodic Wente tori stacked vertically but with a fixed number of unduloid bubbles in between,
- any number of unduloid ends with balanced forces at each bubble,
- any of the previous modifications with nodoid handles (or ends) in place of unduloids.

4. Moduli Spaces of Embedded Symmetric Surfaces with Delaunay Ends

Embedded CMC surfaces with $k \geq 3$ ends and arbitrary genus g exist by the work of Kapouleas [8]. The space $\mathcal{M}_{g,k}$ of these surfaces (modulo motions of 3-space) forms a manifold of dimension $3k-6$ at a non-degenerate surface [13]. This number is independent of the genus and can be interpreted as follows: each end has 3 parameters given by its axis direction and necksize; there is no translational freedom. Kusner's balancing formula (4.1) determines the 3 parameters of one end by those of all others. Finally the rotations of 3-space reduce the dimension further by 3.

In the present section we study subspaces of $\mathcal{M}_{g,k}$ containing the surfaces with some fixed group of reflectional symmetry. The resulting moduli spaces are one- or two-dimensional. The following surprising results are obtained using the algorithm:

- A CMC surface with three ends, one of which is cylindrical (see Figure 4.2.3),
- CMC surfaces with four ends which are all as close to cylindrical as we like, and
- a deformation through CMC surfaces which creates (or deletes) bubbles on a finite length midpiece of a CMC surface.

4.1 Dihedrally Symmetric k-Unduloids

The surfaces with genus 0 and k ends can be considered generalized Delaunay surfaces with k ends and we call them *k-unduloids*. For the special case of k-unduloids with dihedral symmetry $D_k \times \mathbf{Z}_2$ one of us proved existence of a one-parameter family for each $k \geq 3$ [4]; see Figure 4.1 for the symmetric *triunduloids* ($k = 3$). In the family the necksize first monotonically increases from 0 to $1/k$, and then decreases to 0 again. Each such k-unduloid family is a maximal continuous family with the assumed symmetry. Note that the maximal necksize $1/k$ means that the surfaces are the more sphere-like the more ends they have.

In this and more general cases we use the following terminology for the surfaces close to the boundary of the moduli space: we call the surfaces with a central sphere and small necksizes *spheroidal*. To call the surfaces with small necksizes but without central sphere, *noidal*, is justified by the asymptotics of the small central junction: a suitable blow up converges to a minimal k-noid (i.e. a genus 0 minimal surface with k catenoid ends). We would like to mention recent work of Mazzeo and Pacard which could lead to existence proofs of noidal CMC surfaces with genus 0 in general.

As Figure 4.2 shows, embeddedness is not preserved in continuous families of CMC surfaces. Only a generalized notion of embeddedness, *Alexandrov embeddedness*, is preserved; by definition this means that the surface is only immersed but bounds an immersed handlebody. Whereas all the surfaces in

Section 3. are not Alexandrov embedded, we make it a tacit assumption for the remainder.

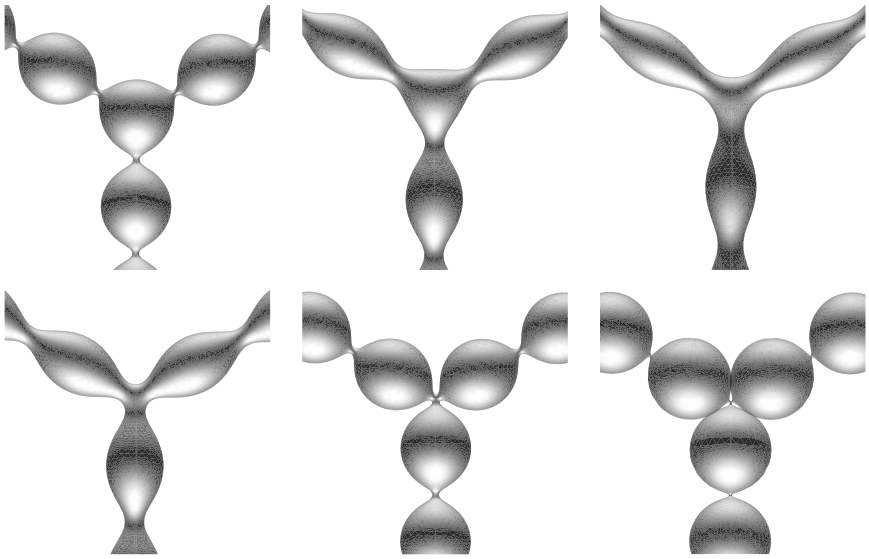

Fig. 4.1. *Six surfaces in the continuous 1-parameter family of triunduloids with dihedral symmetry. The first image is a triunduloid of Kapouleas type with small necks and a spherical central bubble. The maximal necksize* $1/3$ *is reached with the third image. Image four and five have exactly the same necksize as image two and one, respectively, but differ in the central bubble. The trinoidal surface at the end of the family depicted in the sixth image is not embedded any more.*

4.2 Isosceles Triunduloids

By the balancing condition (2.1) the three axes of the ends of a triunduloid lie in a (horizontal) plane. This plane is in fact a symmetry plane for the surface [12]. Here we consider Y-shaped triunduloids with an extra vertical symmetry plane. We call them *isosceles* since they have the symmetry group of an isosceles triangle in 3-space. The intersection of the two symmetry planes gives a line which coincides with the axis of one end, and makes an angle $0 < \alpha < \pi/2$ with each of the other two ends. In particular, the dihedrally symmetric triunduloids are isosceles with $\alpha = \pi/3$.

For isosceles triunduloids (2.1) gives for the necksizes ρ^A of the two arms and ρ^S of the stem

$$\rho^S(1-\rho^S) = 2\cos\alpha\,\rho^A(1-\rho^A). \tag{4.1}$$

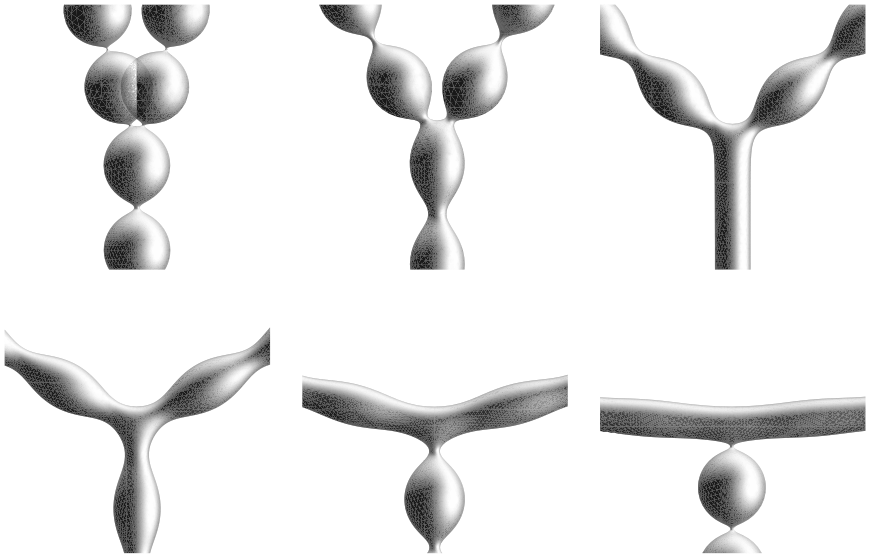

Fig. 4.2. *The one parameter subfamily of isosceles triunduloids which realizes the maximal necksize for a given angle; the images are for the angles* $\alpha = 15,\ 30,$ $\arccos(2/3) \approx 48.2,\ 60,\ 75,$ *and* 85 *degrees. Note the transition from bubble to neck and vice versa on the stem when the cylindrical end is passed.*

Thus α and one necksize can be taken as parameters of the 2-dimensional moduli space.

Experimental Result 5. *There exists a continuous two-parameter family of isosceles triunduloids as follows. Each pair of positive necksizes* ρ^S *of the stem and* ρ^A *of the arms satisfying*

$$\rho^S < \rho^S_{\max}(\alpha) := \min\left\{\frac{\cos\alpha}{2-\cos\alpha},\, 1-\frac{\cos\alpha}{2-\cos\alpha}\right\}, \tag{4.2}$$

or, equivalently,

$$\rho^A < \rho^A_{\max}(\alpha) := \frac{1-\cos\alpha}{2-\cos\alpha}, \tag{4.3}$$

is attained by two different isosceles surfaces of angle α*, whereas the pair* $(\rho^S_{\max}(\alpha), \rho^A_{\max}(\alpha))$ *is attained only once. These are all (Alexandrov embedded) triunduloids with isosceles symmetry.*

In [5], (4.2) and (4.3) are derived as necessary conditions satisfied by all isosceles triunduloids. There is no existence proof yet, and the algorithm is used to this end.

The two degenerate endpoints of each subfamily with fixed α are given by three strings of spheres in isosceles symmetry, in the spheroidal case with

central sphere, in the noidal without. For the angle $\alpha = \arccos(2/3)$ the cylindrical necksize $\rho^S_{\max} = 1/2$ is attained, with $\rho^A_{\max} = 1/4$, see Figure 4.2.3. The arms are never cylindrical but when α tends to $\pi/2$ they can approach the cylinder while the stem tends to a string of spheres (Figure 4.2.6). On the other hand, when $\alpha \to 0$ both ρ^S and ρ^A tend to zero, in fact the maximal necksize $\rho^S_{\max}(\alpha)$ is $\alpha^2/2 + O(\alpha^4)$.

Figure 4.2 indicates a geometric interpretation of the right hand side of (4.2): the two numbers are the two necksizes of the stem, with the minimal necksize being the first expression for $\pi/2 > \alpha \geq \arccos(2/3)$, and the second one for $\arccos(2/3) \geq \alpha > 0$. The necksizes flip their roles exactly at the cylindrical end when they coincide. The same happens if we extend the family of Delaunay unduloids smoothly over the cylinder with the same unduloids translated along their axes by half a period. This observation leads to the following statement, which is obtained from adding (4.2) and (4.3). The subfamily of maximal necksize depicted in Figure 4.2 has necksize sum 1 from the T-shaped up to the cylindrical surface, but necksize sum less than 1 on the way from the cylindrical to the I-shaped surface. However, the sum 1 is also attained on the latter part of the family, if we add the maximal (!) radius of the stem to two times the necksize of the arms.

4.3 Rhombic 4-Unduloids

The X-shaped *rhombic 4-unduloids* have the three orthogonal symmetry planes of a (planar) rhombus in 3-space. We view them as follows: we take an isosceles triunduloid, truncate the stem, and glue a reflected copy onto it. Unlike the isosceles surfaces we do not have a formula at hand which relates the 'necksize' of the midpiece to the necksize of the ends like (4.1), and thus we cannot address the period problem mathematically. Instead we use the numerics to check the period problem.

There are two continuous parameters for rhombic surfaces: the necksize ρ of the 4 ends and the angle $0 < \alpha < \pi/2$ which is defined as for the isosceles case, compare Figure 4.4. For the k-unduloids of genus 1 under the dihedral symmetry group we will see below that the number of bubbles on the finite length midpiece is a (further) discrete parameter which separates connected components of the moduli space; a similar statement holds for various doubly and triply periodic CMC surfaces if their symmetry group is imposed (see [4] [5]).

A surprising result of our experiments is that, on the opposite, each rhombic surface is a continuous deformation (through CMC surfaces) of any other rhombic surface:

Experimental Result 6. *The two-dimensional moduli space of the rhombic 4-unduloids is connected and simply connected.*

Before we discuss the moduli space as represented by Figure 4.3 in detail we give an intuitive reason for the connectedness result, and we discuss a consequence for the general case.

The connectedness is easy to grasp from Figure 4.4: the length of the cylindrical midpiece is a continuous parameter. If we slightly deform its 'necksize' then any number of unduloid bubbles can appear on the midpiece. In this and probably also the general case, the existence of cylindrical pieces in CMC surfaces is crucial to understand the global behaviour of the moduli space.

To draw consequences for the general case $\mathcal{M}_{g,k}$ we go back to the gluing idea. We will see below that the behaviour of the rhombic surfaces is governed by its isosceles junctions, and can be considered a perturbation of the isosceles case with a magnitude exponentially falling in the length of the midpiece. Thus we could say that a rhombic surface consists of two isosceles triple junctions joined with a finite length midpiece. A general k-unduloid can also be considered a union of triple junctions with (more than one) finite length midpieces. Therefore we believe that the rhombic 4-unduloids are general enough to capture the essential behaviour of all k-unduloids, and we expect the connectedness result to carry over to this class.

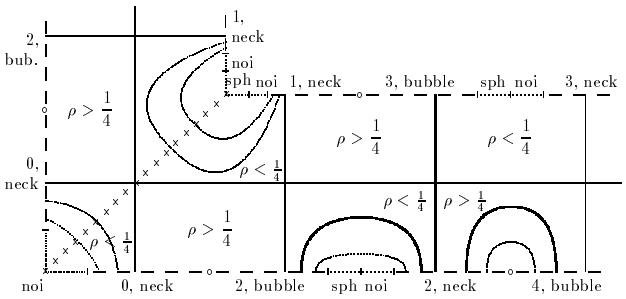

Fig. 4.3. The 2-dimensional moduli space of 4-unduloids with rhombic symmetry is represented with a strip.

4.3.1 Subfamilies of Constant Necksize. We now discuss the moduli space in detail. It turns out that the families of constant necksize ρ are much easier to describe than the families of constant angle α.

The dihedrally symmetric 4-unduloids form a special 1-parameter rhombic subfamily, which is marked with $\times$ in Figure 4.3. These surfaces are fixed points of an automorphism of the rhombic moduli space, namely the rotation by $\pi/2$. This automorphism sends a rhombic surface with angle α to a surface with angle $\pi/2 - \alpha$, and appears in the reflectional symmetry about the diagonal in Figure 4.3. When we divide the (pre)moduli space by the full rhombic isometry group these surfaces should be identified, so that, strictly speaking, only the (half-)strip to one side of the diagonal represents

the moduli space. However, we did not divide by the reflection in Figure 4.3 to simplify following a subfamily across the diagonal.

All necksizes $\rho \in (0, 1/2)$, but $\rho \neq 1/4$, define countably many one-parameter subfamilies; we can consider the number of bubbles on the midpiece the discrete parameter. In Figure 4.3 the curved lines indicate how these families foliate the rhombic moduli space; the two bold curves refer to the families depicted in Color Plate A.2 (p. 19 in the Appendix). However, the necksize $\rho = 1/4$ is a level with branchings; all solid straight lines in Figure 4.3 represent surfaces of this necksize (the surfaces in the middle column of Color Plate A.2 are on the bold straight line).

The degenerate endpoints of the families are given by two Delaunay surfaces connected with a string containing n spheres. If the string is attached to the unduloid bubbles, we include the respective two bubbles in the count of n, if it is attached to the Delaunay necks we do not. This number of bubbles defines countably many subfamilies of constant necksize as follows:

1. For $\rho > 1/4$ they run from $n \in \mathbf{N}_0$ bubbles on the midpiece attached to the unduloid necks, to $n + 2$ bubbles attached to the bubbles; the left column of Color Plate A.2 represents the case $n = 2$.
2. For $\rho = 1/4$ the families represented by the short straight lines in Figure 4.3 run from $n \in \mathbf{N}$ (at neck) to $n+1$ (at bubble); the middle column of Color Plate A.2 illustrates $n = 2$.
3. For $\rho < 1/4$ the number $n \geq 2$ of bubbles on the midpiece is constant; see the right column of Color Plate A.2 for $n = 2$.

For each of the preceding cases the angle α is $\pi/2$, say, at the degenerate endpoints of the family and attains its minimum in $(0, \pi/2)$ exactly when the 'necksize' of the midpiece becomes maximal. The midpiece runs in the x-direction to one side of the dihedrally symmetric 4-unduloids (diagonal in Figure 4.3), and in the y-direction on the other side.

We complete our list with three cases where the diagonal is met:

4. For $\rho = 1/4$ and $n = 0$ there is a surprise: a family runs to infinity along the strip, thereby corresponding to surfaces whose midpiece can have any length. The midpiece is cylindrical and naturally gives rise to a continuous transition to large lengths. This family is represented by the long straight line in Figure 4.3 and some surfaces are given in Figure 4.4. It intersects all families listed in 2 in the surface of minimal angle. Let us point out that the midpiece has a force exceeding that of a cylinder, while its circumference in the vertical symmetry plane equals that of a cylinder, namely $\pi/2$. The dihedrally symmetric 4-unduloid of maximal necksize ($\rho = 1/4$) satisfies this property with respect to both vertical symmetry planes.
5. For $\rho < 1/4$ and $n = 1$ bubble on the midpiece, the family meets the dihedrally symmetric 4-unduloids of spheroidal type.

6. And for $\rho < 1/4$ and $n = 0$ bubbles on the midpiece, the family meets the dihedrally symmetric 4-unduloids of noidal type.

The cases 1 to 3 follow for large n from the analysis of the isosceles case given in [5] in the following way. Let us define the necksize ρ^S of the midpiece by its circumference (over 2π) in the vertical symmetry plane. In the limit of long midpieces the necksizes ρ^S, $\rho^A := \rho$ satisfy (4.1), since if we fix one triple junction of a rhombic surface the limit is an isosceles surface. However for finite lengths the influence of the different period problem for the rhombic case results in a deviation from (4.1). If we assume this deviation is continuous in the length of the midpiece, then indeed we can carry out an analysis of the boundary contours similar to the isosceles case [5] which yields Figure 4.3 in a neighbourhood of infinity.

Numerically we could not distinguish our parameters ρ and α in case 1 to 3 from their values for the respective isosceles surfaces. However, in case 4 we observed that α is significantly different from the isosceles cylindrical value $\arccos(2/3)$. Three known values of α support the experimental findings:

- When the length of the midpiece tends to 0 the surfaces converge to two parallel Delaunay unduloids of necksize $1/4$, tangent (with opposite normals) at points of minimal radius at their necks. Since the axes are parallel $\alpha \searrow 0$; compare to Figure 4.4.1.
- The symmetric 4-unduloid has $\alpha = \pi/4$; see Figure 4.4.2.
- When the length of the cylindrical midpiece tends to infinity the limit is the isosceles surface with cylindrical end. Therefore, $\alpha \nearrow \arccos(2/3)$; compare to Figure 4.4.3.

We interpolated these values of α with an exponential function. This approximates the actual function up to an error which was smaller than what the numerical scheme can distinguish. It is also conceivable that α is monotonic in cases 5 and 6, but we did not conduct numerical experiments.

4.3.2 The Boundary of the Moduli Space. The boundary is the space of limits of rhombic surfaces with respect to Hausdorff distance taken on compact sets of 3-space. In the limit necks pinch off so that the limiting surface decomposes into (strings of) spheres and Delaunay unduloids. There are two connected boundary components containing the following geometrically different degenerate surfaces. They repeat cyclically on the boundary with different numbers of bubbles n on the midpiece.

1. Ends and midpiece consist of spheres ($\rho = 0$). There are two junction spheres, to which midpiece and ends are attached. The midpiece consists of $n \in \mathbf{N}$ spheres (including the junction spheres in the count). These surfaces are limits of spheroidal rhombic surfaces, and are marked with a dotted line and a 'sph' in Figure 4.3. The angle $\alpha \in [0, \pi/2]$ is a parameter.

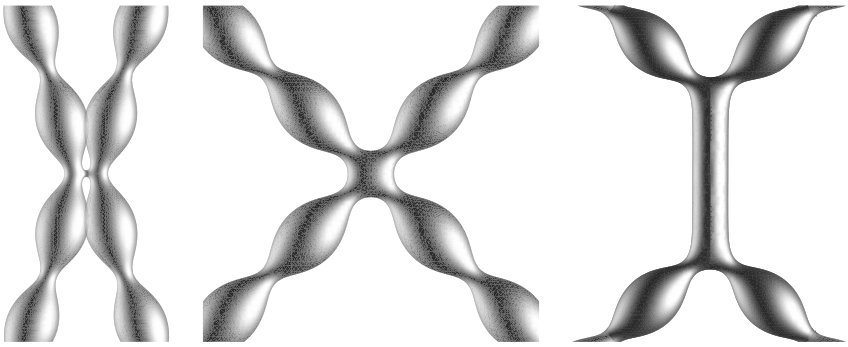

Fig. 4.4. *A special one-parameter subfamily of rhombic surfaces with necksize* $1/4$ *is given by the surfaces with cylindrical midpiece. On all images the midpiece runs in the y-direction; it is short for the first picture which is close to two unduloids joined with a small neck* ($\alpha = 0$). *The second image is the symmetric 4-unduloid of maximal necksize with* $\alpha = \pi/4$. *In the third image the length is larger, and the angle approaches its isosceles value* $\arccos(2/3)$.

2. Again ends and midpiece are spheres ($\rho = 0$). However, now the midpiece of $n \in \mathbf{N}_0$ spheres meets the ends come in a trinoidal junction. This case is marked with a dotted line and a 'noi' in Figure 4.3, and can again be parameterized by $\alpha \in [0, \pi/2]$.
3. Two unduloids of necksize $\rho \in (0, 1/2]$ enclose a spherical midpiece with $n \in \mathbf{N}_0$ spheres. The midpiece is attached to the unduloid necks. These surfaces with angle $\alpha = \pi/2$ (or 0) are represented with dashed lines in Figure 4.3, and labeled 'n, neck'. The first row of Color Plate A.2 gives surfaces closeby.
4. As the preceding case, but now the midpiece is attached to the unduloid bubbles; it contains $n \geq 2$ bubbles (including the 2 unduloid bubbles). These surfaces are labeled with 'n, bubble' in Figure 4.3, and closeby surfaces are given in the bottom row of Color Plate A.2.

Consecutive cases have a degenerate surface in common: 1. and 2. coincide in a straight surface with $\alpha = 0$ (or $\pi/2$), which has two opposite strings of spheres with multiplicity 2; the junction sphere of 1. is the first sphere of the midpiece in 2. Case 2. coincides with 3., as does 4. with 1., in the case that the unduloid degenerates to a string of spheres. Finally 3. and 4. have the case of a cylindrical unduloid, $\rho = 1/2$, in common; it is marked with a circle in Figure 4.3. Since we include the unduloid bubble (but not the necks) in our count of bubbles on the midpiece, the number jumps by two at these cylindrical surfaces. This leads to the fact that one boundary contains surfaces with an even number of spherical bubbles on the midpiece while the other contains an odd number.

4.4 Dihedrally Symmetric k-Unduloids of Genus 1

No 2-unduloids of genus 1 exist [12] and so we assume $k \geq 3$. The *(dihedrally symmetric) k-unduloids of genus 1* are similar to reflected isosceles surfaces truncated at their arms, with an angle $\alpha = \pi/2 - \pi/k$. As in the rhombic case we need the numerical algorithm to handle the period problem. We computed some triunduloids and 4-unduloids of genus 1, see Figure 4.5.

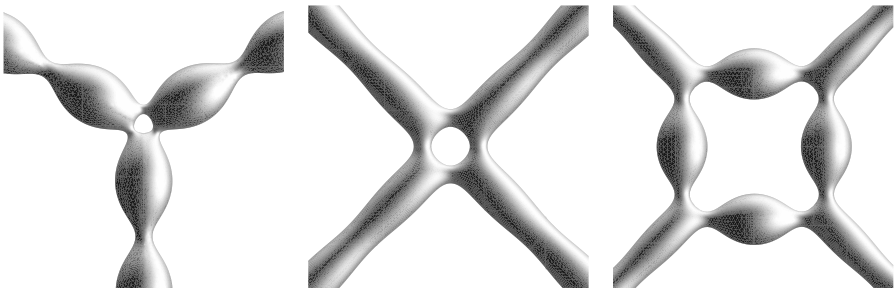

Fig. 4.5. *Dihedrally symmetric k-unduloids of genus 1. The first image is a genus 1 triunduloid of maximal necksize. The other two images display two different 4-unduloids of maximal necksize: one with no extra bubble on the finite length piece, the other with one extra bubble. The necksize of the left 4-unduloid is slightly larger than that of right.*

As pointed out before the number of bubbles on the midpiece separates connected components of the moduli spaces, each given by a continuous 1-parameter family. We do not yet know whether or not these families are connected by genus 1 k-unduloids without the dihedral symmetry assumption.

Experimental Result 7. *There are countably many continuous 1-parameter families of dihedrally symmetric k-unduloids of genus 1, distinguished by the integer number n of bubbles on the finite length pieces. Some maximal necksize $\rho_{\max}(k,n)$ of the ends is attained by one surface, whereas each smaller necksize is attained twice. Furthermore,* $\lim_{n\to\infty} \rho_{\max}(k,n) = \rho^S(\pi/2 - \pi/k)$.

The proof that the limit of the maximal necksizes converges to the maximal necksize of isosceles stems is as follows: fixing one triple junction and increasing the number of bubbles on the finite length pieces gives an isosceles triunduloid as the limit. From an analysis similar to [5] it follows that $\rho_{\max}(k,n)$ is decreasing for increasing n and fixed k. The dependence turned out to be tiny however, and we could not detect it by our numerical experiments.

For $k = 3$ the maximal necksize of the ends is at about $\rho^S_{\max}(\pi/6) \approx 0.236$. For $k = 4$ we are closer to the cylindrical end with $\rho^S_{\max}(\pi/4) \approx 0.453$.

Starting with $k \geq 4$ the maximal necksize decreases monotonically in k (for a given number of bubbles). The range of necksizes is remarkably different for the genus 0 and genus 1 cases (we always consider the limit of many bubbles on the finite length pieces):

- The necksize sum is at most 1 in the genus 0 case, but is $4\rho^S_{\max}(\pi/4) \approx 1.81$ for the genus 1 case with 4 ends.
- The necksize is maximal at $k = 3$ for genus 0, but at $k = 4$ for genus 1.
- As $k \to \infty$ the necksize is at most $1/k$ for genus 0, but by (4.2) it is at most $1/(2k)$ for genus 1.

References

1. U. Abresch, *Constant mean curvature tori in terms of elliptic functions*, J. Reine Angew. Math. **374** (1987), 169–192.
2. A. Bobenko, *All constant mean curvature tori in R^3, S^3, H^3 in terms of theta functions*, Math. Ann **290** (1991), 209–245.
3. C. Delaunay, *Sur la surface de révolution, dont la courbure moyenne est constante*, J. Math. Pures Appl. **6** (1841), 309–315.
4. K. Grosse-Brauckmann, *New surfaces of constant mean curvature*, Math. Zeit. (1993), 527–565.
5. K. Grosse-Brauckmann and R. Kusner, *Moduli space of embedded constant mean curvature surfaces with few ends*, in preparation.
6. K. Grosse-Brauckmann and K. Polthier, *Numerical examples of compact surfaces of constant mean curvature*, Elliptic and Parabolic Methods in Geometry (B. Chow, R. Gulliver, S. Levy, and J. Sullivan, eds.), A K Peters, Wellesley (MA), 1996, pp. 23–46.
7. ———, *Compact constant mean curvature surfaces with low genus*, Experim. Math. (to appear 1996).
8. N. Kapouleas, *Complete constant mean curvature surfaces*, Ann. of Math. **101** (1990), 239–330.
9. ———, *Compact constant mean curvature surfaces in euclidean three-space*, J. Diff. Geom. **33** (1991), 683–715.
10. ———, *Constant mean curvature surfaces constructed by fusing Wente tori*, Invent. Math. **64** (1995), 443–518.
11. H. Karcher, *The triply periodic minimal surfaces of A. Schoen and their constant mean curvature compagnions*, Man. Math. **64** (1989), 291–357.
12. N. Korevaar, R. Kusner, and B. Solomon, *The structure of complete embedded surfaces with constant mean curvature*, J. Diff. Geom. **30** (1989), 465–503.
13. R. Kusner, R. Mazzeo, and D. Pollack, *The moduli space of complete embedded constant mean curvature surfaces*, Geom. Funct. Anal. **6** (1996), 120–137.

14. H. Lawson, *Complete minimal surfaces in S^3*, Ann. of Math. **92** (1992), 335–374.

15. R. Mazzeo and D. Pollack, *Gluing and moduli for non-compact geometric problems*, preprint (1996).

16. B. Oberknapp and K. Polthier, *An algorithm for discrete constant mean curvature surfaces*, Visualization and Mathematics (H.-C. Hege and K. Polthier, eds.), Springer Verlag, 1996

17. U. Pinkall and I. Sterling, *On the classification of constant mean curvature tori*, Ann. of Math. **130** (1989), 407–451.

18. H. Wente, *Counterexample to a conjecture of H. Hopf*, Pac. J. of Math. **121** (1986), 193–243.

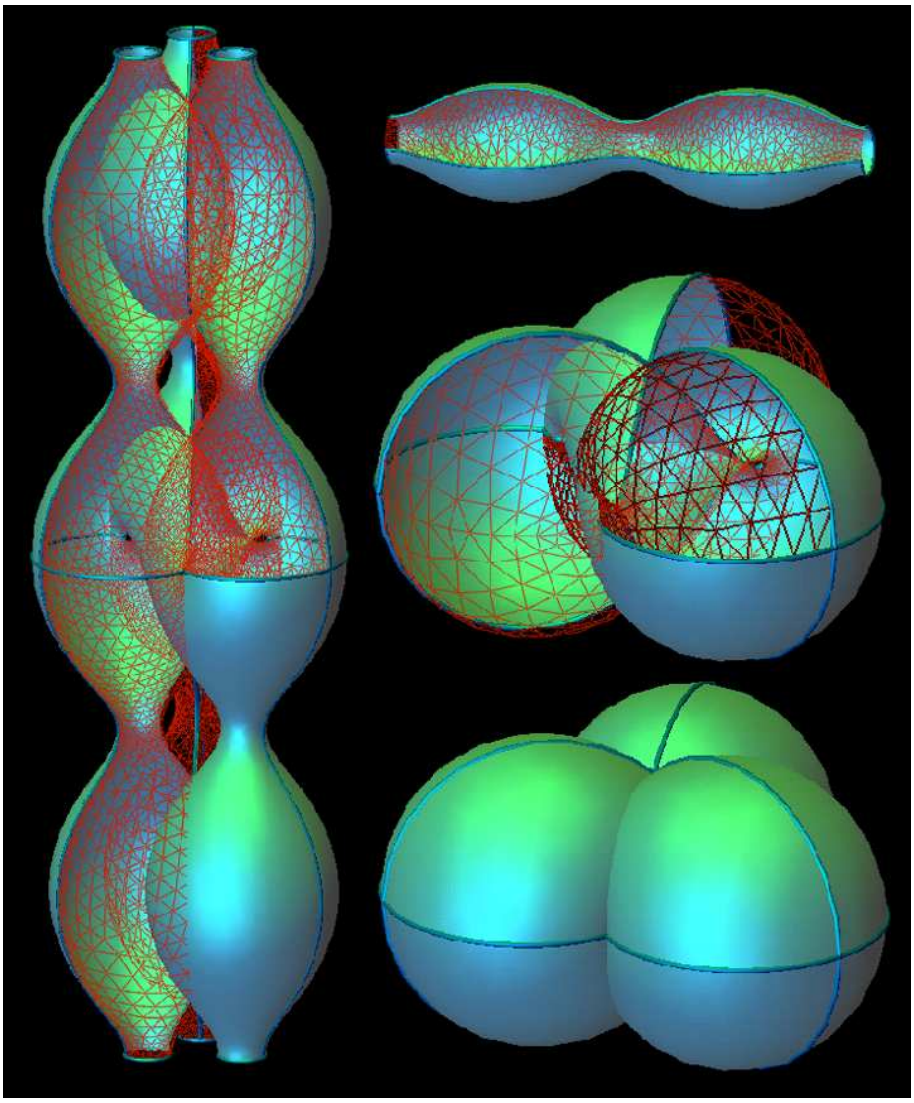

Fig. A.1. *Modification of the Wente torus by attaching six Delaunay unduloid ends. The result is a genus one constant mean curvature surface (left). The six ends have parallel axes. The images on the right explain the building blocks used in the construction: two bubbles of a rotationally symmetric Delaunay unduloid, and two views of a Wente torus - two quadrilateral fundamental domains are shown as grid.*

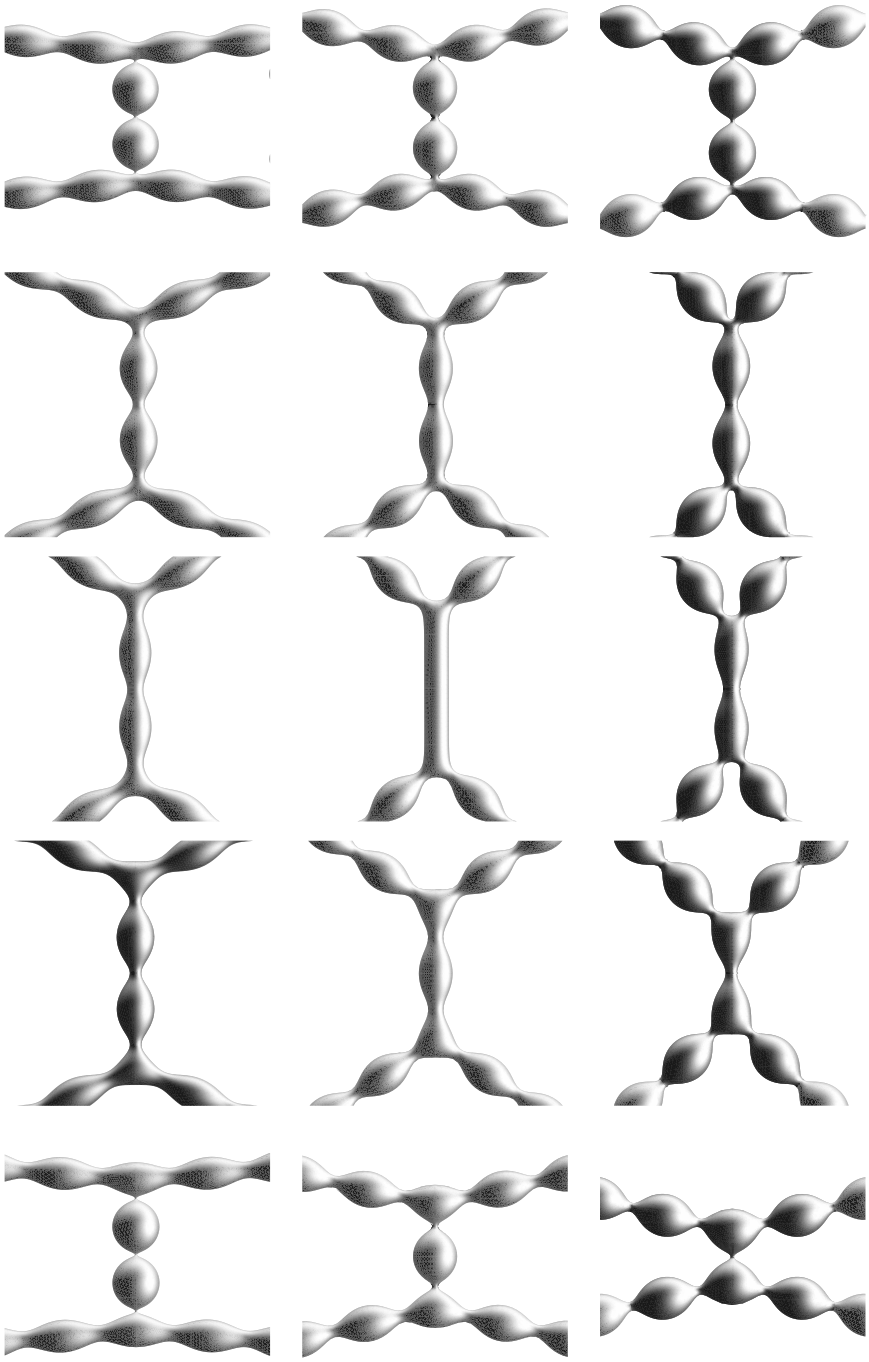

Fig. A.2. *Constant mean curvature surfaces with four unduloid ends and genus 0. The shown two-parameter family has the symmetry of a planar rhombus and we therefore we call the surfaces rhombic. The columns represent one-parameter subfamilies with fixed necksize* 1/3, 1/4, 1/6, *respectively. Note that in each column a different number of bubbles on the midpiece is created. This behaviour can be closely related to the fact that a cylindrical midpiece can occur (middle picture) where the necksizes flip their roles.*